



## Biosorption Potential of *Saraca asoca* Bark Powder for Removal of Cr (VI) Ions from Aqueous Solution

Anurag Samson Lall<sup>1\*</sup>, Avinash Kumar Pandey<sup>2</sup> and Jyoti Vandana Mani<sup>1</sup>

1. Department of Chemistry, Sam Higginbottom University of Agriculture, Technology and Sciences, Prayagraj, Uttar Pradesh, 211007, India
2. Department of Chemistry, GLA University, Chaumuhan, Mathura, Uttar Pradesh, 281406, India

Received: 21.08.2021, Revised: 15.10.2021, Accepted: 24.11.2021

### ABSTRACT

*Saraca asoca* bark has long been used in traditional Indian medicine. Considering its low cost and non-toxic nature, it can find application as a biosorbent. This article explores the application of *Saraca asoca* bark powder (SABP) for biosorption of hexavalent chromium. Various analytical techniques including Field emission scanning electron microscope (FESEM) attached with energy dispersive spectrometer (EDS), Fourier transform infrared spectroscopy (FTIR) and point of zero charge ( $\text{pH}_{\text{pzc}}$ ) were adopted in order to identify the physico-chemical features of SABP. Factors such as pH (2-8), contact time (for 3 hours), initial Cr (VI) concentration (10 – 250 mg/l) and temperature (15 - 35°C) were examined for their influence on Cr (VI) biosorption via batch studies. Biosorption data clearly followed Redlich-Peterson isotherm model as compared to Langmuir and Freundlich models. The Langmuir monolayer adsorption capacities ( $Q_m$ ) at 15, 25 and 35°C were 123.4, 125.0 and 175.4 mg/g respectively. Biosorption followed pseudo-second-order kinetics and the mechanism of diffusion was governed by both surface sorption and pore diffusion as demonstrated by the plot for Intraparticle diffusion model and the pore diffusion coefficient ( $D_p \sim 10^{-9} \text{ cm}^2/\text{s}$ ). The nature of biosorption was found to be spontaneous and endothermic as reflected through various thermodynamic parameters such as the free energy change ( $\Delta G = -3.0$  to  $-3.7 \text{ kJ/mol}$ ), entropy change ( $\Delta S = 37.8 \text{ J/K/mol}$ ) and enthalpy change ( $\Delta H = 7.9 \text{ kJ/mol}$ ). The study recommends that SABP may be utilized as a potential biosorbent for Cr(VI) ions.

**Keywords:** Tree bark, Biosorbent, Hexavalent chromium, Heavy metal, Batch studies

### INTRODUCTION

Heavy metal contamination of water resources is one of the world's major challenges, posing significant environmental risk. Since chromium is involved in a number of industrial processes, including leather tanning, textile dyeing, wood processing, metal refining as well as in cement and steel industries, it is often responsible for contamination of surface water (Hadjmohammadi *et al.*, 2011). Chromium occurs in aqueous environments in trivalent ( $\text{Cr}^{3+}$ ) as well as hexavalent ( $\text{Cr}^{6+}$ ) states, amongst which the former is less toxic. At lower concentrations Cr(III) serves as an important micro-nutrient for mammals, however the Cr(VI) form is nearly 500-fold more hazardous than Cr(III). Chromium (III) sulfate is frequently used in leather tanning industries, because it is relatively cheap and facilitates high operative speed, enhanced stability and higher mechanical strength. (Gebrehawaria *et al.*,

\* Corresponding Author Email: anuragsam7son@gmail.com

2014). The Cr(III) ions thus released as tannery waste, easily oxidize to Cr(VI) form, posing significant environmental concern (Sarin & Pant, 2006).

Cr(VI) is carcinogenic, mutagenic and teratogenic in nature (Alemu *et al.*, 2018). Consumption of Cr(VI) contaminated water has been associated with increased onset of several ailments in human beings including nausea, diarrhea, vomiting, gastrointestinal ulcers, liver damage and various carcinomas (Gebrehawaria *et al.*, 2014). Therefore Cr(VI) has been recognized by the United States Environmental Protection Agency (USEPA) as a high priority hazardous pollutant (Ma *et al.*, 2014; Zhou *et al.*, 2016). As per the World Health Organization (WHO), the permissible limit for Cr(VI) in drinking water is 0.05 ppm (Alemu *et al.*, 2018). Similarly, the maximum threshold for Cr(VI) discharge in industrial effluents has been restricted to 0.1 ppm by the Indian government (Bhattacharya *et al.*, 2008). In order to comply with these permissible limits, the industrial effluents must be suitably treated so as to ensure adequate reduction in chromium concentration.

Although, several techniques such as membrane separation, ion exchange, microbial action, chemical precipitation and adsorption have been used for mitigation of Cr(VI) contamination, the adsorption method provides an effective and flexible approach due to high selectivity, economic effectiveness and ease of implementation (Mutongo *et al.*, 2014; Zhou *et al.*, 2016). Recently immense interest has emerged towards use of different biomaterials as adsorbents. Commonly used biosorbents include inexpensive agricultural wastes and byproducts such as wheat bran, tobacco stem, rice husk, coffee husk, citrus peels and potato peels etc. (Sud *et al.*, 2008; Yuvaraja *et al.*, 2014; Saxena *et al.*, 2017). Such materials contain lignin, cellulose and hemicellulose as major components which are known to form complexes with metal ions (Ofomaja & Ho, 2007).

*Saraca asoca* is an evergreen tree which belongs to the family “Fabaceae” and is found in different parts of India, Bangladesh, Myanmar, Sri Lanka and Malaysia. In India, it is locally known as ‘Ashoka’ and is considered an important and sacred tree. Different parts of this tree including bark, leaves, flowers and seeds are often used in traditional Indian medicine (Smitha & Thondaiman, 2016). Its bark is dark brown in colour, bitter and astringent in taste, is non-toxic (Mukhopadhyay & Nath, 2011; Ahmad *et al.*, 2016) and is used in several ayurvedic preparations for treating different feminine disorders and gynecological problems. To the best of our knowledge, *Saraca asoca* bark has not been reported to be used as an adsorbent for removal of heavy metal ions. This manuscript therefore examines the applicability of *Saraca asoca* bark powder (SABP) as a biosorbent for remediation of Cr(VI) contamination, discussing the nature and morphology of the adsorbent, its mechanism of interaction, adsorption kinetics, thermodynamics as well as equilibrium isotherms.

## MATERIALS AND METHODS

The analytical grade reagents and chemicals used during the study were brought from E. Merck, India Ltd. Drying of the adsorbent was accomplished using Hot Air Oven (Model IIC-101, Impact - Icon Instruments, New Delhi, India). The batch adsorption study was carried out using Orbital shaker – BOD incubator (Model IIC-119A, Impact - Icon Instruments, New Delhi, India). Similarly pH of the adsorbate solution was measured using pH meter (Labtronics, Panchkula, Haryana, India).

2.829 g of potassium dichromate (Assay 99.8%) was dissolved in 1 liter double distilled water to obtain a stock solution of 1g/l Cr(VI) ions (Campaña-Pérez *et al.*, 2019; Tao *et al.*, 2020). This solution was further diluted to prepare chromium (VI) solutions of 10, 50, 100, 150, 200 and 250 ppm concentrations. The pH of the solution was adjusted to desired value by adding 0.01M HCl or NaOH as per the requirement.

The *Saraca asoca* bark was procured from the premises of St. Andrew's Church, Gorakhpur, Uttar Pradesh, India (26°45'46.674"N, 83°23'28.2012"E). The collected bark was thoroughly washed with distilled water, dried in sunlight and then cut into small pieces. These pieces were further completely dried in hot air oven followed by grinding in a hammer mill to obtain a powder which was sieved to particle size 90 – 125 µm. For avoiding the discharge of coloured matter in the aqueous medium, the water soluble components were removed by soxhlet extraction with hot water using solid-liquid ratio 1:10 (g/ml) at 50°C for 4 hours (Saliba *et al.*, 2002; Litefti *et al.*, 2019; Kavitha & Kandasubramanian, 2020). The obtained material was then dried in hot air oven at 70°C, cooled and stored in air tight plastic bottles till further study.

The changes in surface morphology and elemental composition of SABP after Cr(VI) loading was explored using Field Emission Scanning Electron Microscope coupled with Energy Dispersive Spectrometer (FESEM-EDS) and Au Sputter Coater (JEOL JSM – 7610F Plus OXFORD EDS) with 15kV accelerating voltage and 5nA probe current using a back scattered electron detector. The characteristic functional groups over the surface of SABP, before and after the adsorption were identified with help of Fourier Transform Infrared Spectrometer (FTIR) with Diamond ATR (Perkin Elmer Spectrum 2) in the scan range 400 – 4000 cm<sup>-1</sup> with 1 cm<sup>-1</sup> resolution and 32000:1 sensitivity. For this purpose, the adsorbent was mixed with KBr in 1:50 (mg/mg) ratio and pressed in the form of pellet (Litefti *et al.*, 2019).

The pH value at point of zero charge (pH<sub>pzc</sub>) for the SABP was determined using batch equilibrium study (Lazarević *et al.*, 2007; Alemu *et al.*, 2018; Mohebbali *et al.*, 2019). 0.5 g of SABP adsorbent was taken in each of 7 conical flasks and 50 ml of 0.01 M KNO<sub>3</sub> solution was added to each flask. The initial pH (pH<sub>i</sub>) of the mixtures were adjusted to values 2 to 8. These flasks were then agitated at 140 rpm in a BOD incubator orbit shaker maintained at 25°C for 8 hours. The final equilibrium pH values (pH<sub>f</sub>) were carefully recorded. The ΔpH (pH<sub>f</sub> – pH<sub>i</sub>) was plotted as a function of pH<sub>i</sub> and the intercept at x – axis was reported as pH<sub>pzc</sub> value.

200 ml of Cr(VI) solution of desired concentration was taken in conical flasks. The pH of the solutions in each of these flasks were adjusted to required values followed by addition of 100 mg of SABP. These flasks were then placed in a BOD incubator orbit shaker at 140 rpm speed and suitable temperature. Different sets of batch experiments were performed by varying different parameters including pH, Cr(VI) concentration, contact time and temperature. Finally the mixtures were filtered using Whatman filter paper no. 42 and the concentration of Cr<sup>6+</sup> ions in the filtrate solution was determined with help of Atomic Absorption Spectrophotometer (Analytic Gena, Model AAS 5EA) at 357.9 nm using 0.7 nm slit width. The adsorption capacity at any instant time t (Q<sub>t</sub>) and percentage removal (%R) were calculated with help of following equations:

$$Q_t = \frac{(C_0 - C_t) \times V}{W} \quad \text{and} \quad \%R = \frac{(C_0 - C_t) \times 100}{C_0}$$

where C<sub>0</sub> and C<sub>t</sub> are Cr(VI) ion concentrations initially and at any particular instant of time t respectively. Similarly W and V are the amount of adsorbent used in grams and the volume of solution being tested in liters.

The obtained adsorption data was examined using Langmuir, Freundlich and Redlich-Peterson adsorption isotherms as well as pseudo – first order, pseudo – second order and intra particle diffusion kinetic models. The deviation between the predicted model data and the observed experimental data was evaluated using Pearson's Chi – square test for goodness of

fit which reflects the sum of squared differences between the experimental and predicted data (Dada *et al.*, 2020). The  $\chi^2$  value was calculated using following formula:

$$\chi^2 = \Sigma \frac{(\text{observed value} - \text{predicted value})^2}{\text{predicted value}}$$

## RESULTS AND DISCUSSION

Field emission scanning electron microscope (FESEM) is utilized as an important tool to analyze variations in the surface morphology of the adsorbent. It identifies the possible active sorptive sites and reveals important data regarding the porosity and the overall surface texture. **Figure 1** displays the FESEM micrographs of SABP before and after loading  $\text{Cr}^{6+}$  ions at 3000 magnification.

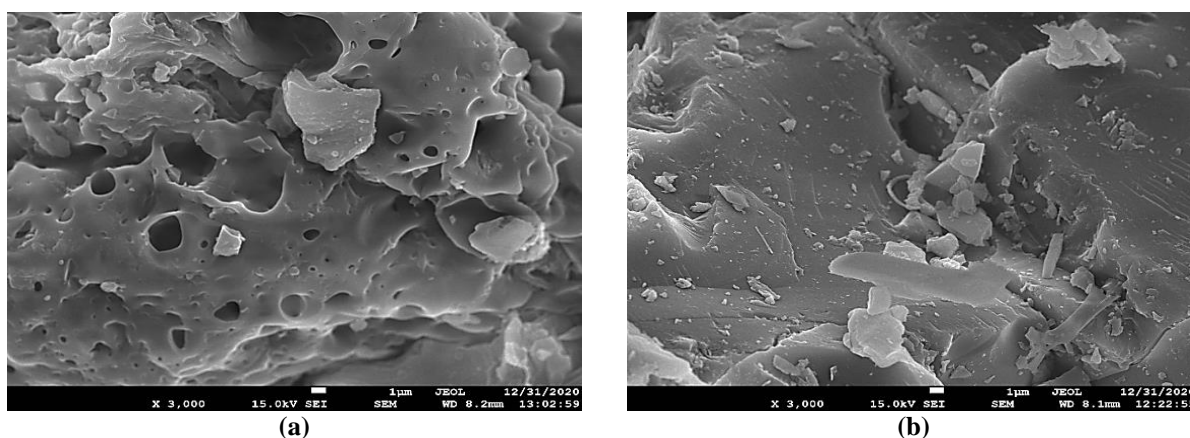


**Fig 1.** FESEM images of SABP adsorbent (a) before and (b) after adsorption of  $\text{Cr}^{6+}$  ions.

It is clear from the figure that the  $\text{Cr}^{6+}$  adsorption altered the morphology of the SABP surface. Initially the SABP surface exhibited an uneven and irregular texture with multiple pores of varied shapes and sizes. However after  $\text{Cr}^{6+}$  adsorption, the surface appears to be covered with layer of  $\text{Cr}^{6+}$  ions covering all the pores, implying that the pores had sufficient dimensions to ensure penetration of  $\text{Cr}^{6+}$  ions.

The analytical technique Energy dispersive x – ray analysis (EDS) uses X – ray excitation of a substance so as to examine its chemical composition. Each element produces a unique set of peaks in the x – ray emission spectrum. **Figure 2** shows the EDS spectra and corresponding elemental loadings of SABP before and after  $\text{Cr}^{6+}$  adsorption.

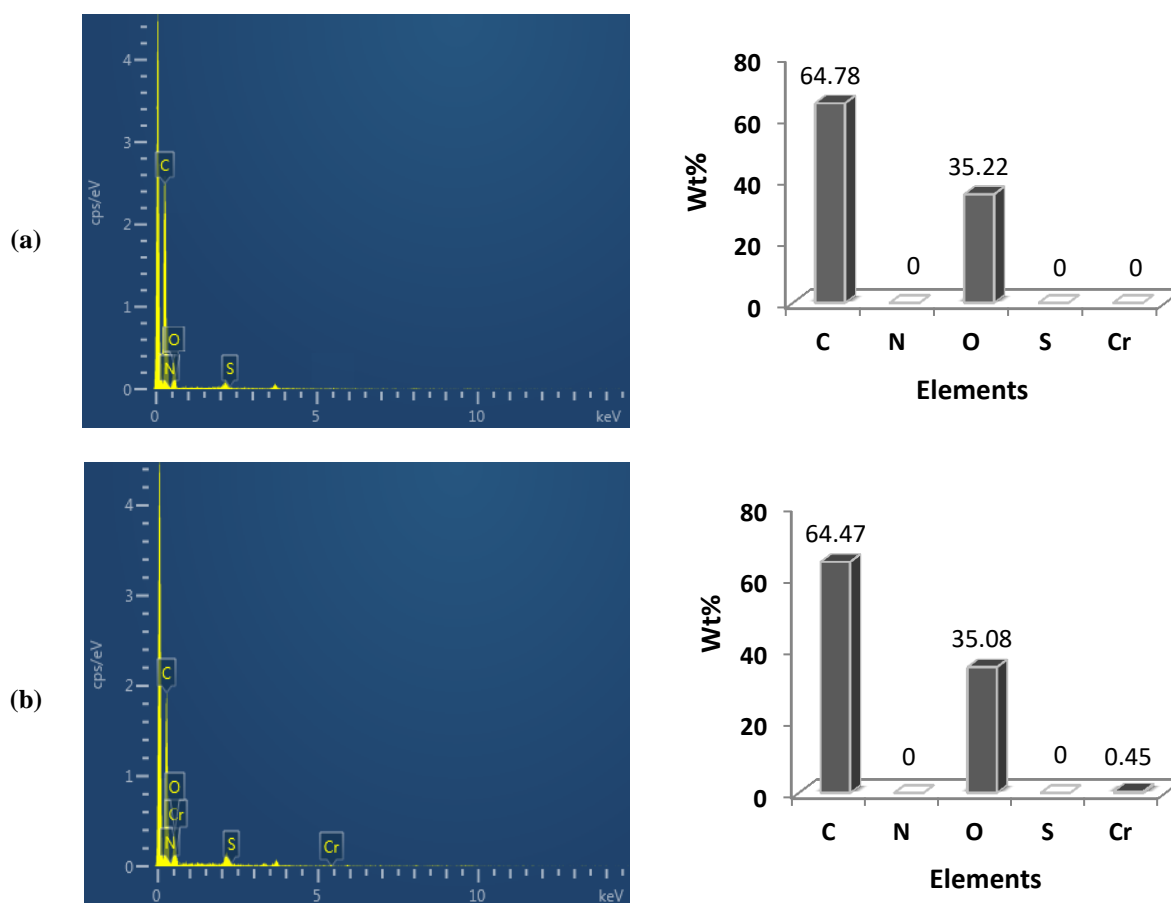


**Fig 2:** EDS spectra and elemental loadings of (a) SABP adsorbent and (b) SABP adsorbent loaded with  $\text{Cr}^{6+}$  ions.

The EDS analysis suggests that SABP contains C, 64.78% and O, 35.22% (%w/w) as major elements which is characteristic for lignocellulosic materials (Litefti *et al.*, 2019). The biosorption of  $\text{Cr}^{6+}$  was revealed by appearance of peaks at 0.57, 5.4 and 5.9 keV (Karthik & Meenakshi, 2014; Ajmani *et al.*, 2019).

Fourier Transform Infrared Spectra (FT-IR) helps in examining the organic functional groups of the biosorbent surface which interact with the metal ions (Wang & Chen, 2009; Chen *et al.*, 2010). Figure 3 depicts the FTIR spectra of SABP before and after  $\text{Cr}^{6+}$  loading. The corresponding assignment of peaks has been illustrated in Table 1.

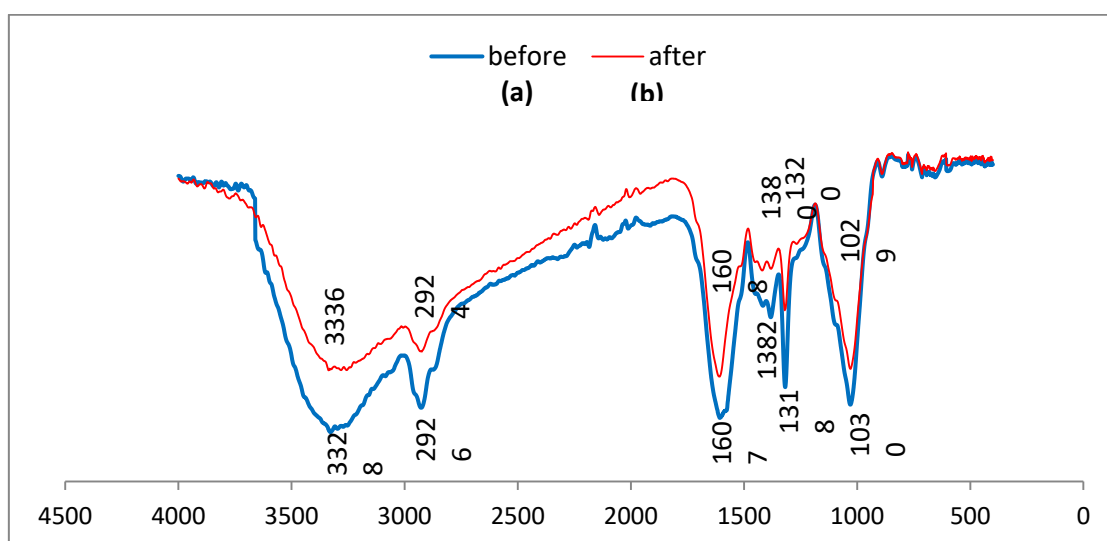


**Fig 3:** FTIR spectra of (a) SABP adsorbent and (b) SABP adsorbent loaded with  $\text{Cr}^{6+}$  ions.

**Table 1:** Assignment of FTIR peaks for adsorbent SABP before and after adsorption of  $\text{Cr}^{6+}$  ions.

Frequency ( $\text{cm}^{-1}$ )		Assignment of peak	Reference
SABP	Cr(6+) loaded SABP		
3328	3336	O-H stretching	Mustapha <i>et al.</i> , 2019
2926	2924	methyl C-H asymmetric stretching	Fuks <i>et al.</i> , 2006
1607	1608	conjugated C=C	Coates, 2000
1382	1380	methyl C-H symmetric bending	Politi & Sidiras, 2020
1318	1320	O-H in plane bending	Coates, 2000
1030	1029	C-O stretching	Chen <i>et al.</i> , 2010

It is evident from the table that the major surface functional group appears to be the  $-\text{OH}$  group with absorption peaks at 3328 (broad), 1318 and 1030  $\text{cm}^{-1}$  representing the O-H stretching (Mustapha *et al.*, 2019), O-H in plane bending (Coates, 2000) and C-O stretching (Chen *et al.*, 2010) respectively. Similarly, the peaks at 2926 and 1382  $\text{cm}^{-1}$  reveal C-H asymmetric stretching (Fuks *et al.*, 2006) and C-H symmetric bending (Politi & Sidiras, 2020) respectively, suggesting the existence of methyl group. The peak at 1607  $\text{cm}^{-1}$  may indicate conjugated C=C bond (Coates, 2000). Biosorption of  $\text{Cr}^{6+}$  ions caused a major blue shift in O-H stretching frequency from 3328 to 3336  $\text{cm}^{-1}$  and O-H in plane bending frequency from 1318 to 1320  $\text{cm}^{-1}$  which may be associated with the presence of hydroxyl groups in lignin, cellulose and hemicellulose (Politi & Sidiras, 2020). Similarly red shift was observed in frequencies from 2926 and 1382  $\text{cm}^{-1}$  to 2924 and 1380  $\text{cm}^{-1}$  respectively. Besides the shift in frequencies, a substantial decrease in peak intensities was observed in FTIR spectra of SABP after  $\text{Cr}^{6+}$  loading (Chen *et al.*, 2010).

At a particular pH, the overall charge on the biosorbent surface may be realized in terms of the point of zero charge (pzc). At point of zero charge, the pH value ( $\text{pH}_{\text{pzc}}$ ) represents the condition, when the magnitudes of positive and negative charges over the adsorbent's surface become equal. Typically the surface functional groups of adsorbent acquire an overall charge which is contingent on the pH of the solution (Omorogie *et al.*, 2016). It is known that at  $\text{pH} < \text{pH}_{\text{pzc}}$ , an overall positive charge is induced over the adsorbent surface however at  $\text{pH} > \text{pH}_{\text{pzc}}$  the surface acquires a negative charge (Alemu *et al.*, 2018; Gómez-Aguilar *et al.*, 2021). The  $\text{pH}_{\text{pzc}}$  for SABP was obtained as 5.5 via batch equilibrium study by plotting change in pH ( $\Delta\text{pH}$ ) as a function of initial pH ( $\text{pH}_i$ ) (Figure 4a).

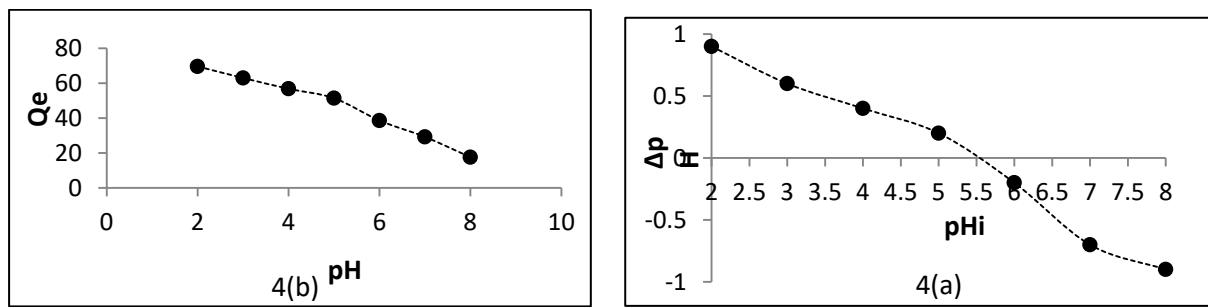


**Fig 4.** (a) Plot of change in pH ( $\Delta\text{pH}$ ) versus initial pH ( $\text{pH}_i$ ) and (b) Effect of pH on adsorption of  $\text{Cr}^{6+}$  ions on SABP adsorbent.

It is eminent that in acidic conditions,  $\text{Cr}^{6+}$  mainly exists as negatively charged hydrogen chromate ion ( $\text{HCrO}_4^-$ ), while at higher pH, it forms chromate ion ( $\text{CrO}_4^{2-}$ ) (Pakade *et al.*, 2017). **Figure 4b** displays the plot of equilibrium adsorption capacity ( $Q_e$ ) versus pH of the solution. The figure clearly denotes that as the pH decreases (from pH = 5 to 2),  $Q_e$  increases gradually, however it decreases sharply as the pH increases (from pH = 5 to 8). This observation can be interpreted with help of  $\text{pH}_{\text{pzc}}$ . At  $\text{pH} < 5.5$  ( $\text{pH}_{\text{pzc}}$ ), the SABP surface is predominantly positively charged, causing substantial electrostatic attraction towards  $\text{HCrO}_4^-$  ion, resulting in enhanced adsorption capacities. However at  $\text{pH} > 5.5$  ( $\text{pH}_{\text{pzc}}$ ), the adsorption capacities are significantly reduced because of electrostatic repulsion between negatively charged chromium species and the SABP surface. Additionally, the competition between the hydroxyl ions and the negatively charged chromium species may also have a major contribution (Alemu *et al.*, 2018).

**Table S1** illustrates complete data for biosorption of  $\text{Cr}^{6+}$  over SABP at varied conditions including changes in pH, initial chromium concentration, contact time and temperature. **Figure 5** displays plot of adsorption capacity versus contact time at different initial  $\text{Cr}(\text{VI})$  concentrations as well as plot of adsorption capacity versus initial  $\text{Cr}(\text{VI})$  concentration at varied temperatures. Initially due to availability of vacant sites, the adsorption capacity increased rapidly with time; however as the sites began to fill, it gradually decreased till it reached the equilibrium (Yuvaraja *et al.*, 2014). Similarly, the equilibrium adsorption capacity increased with increase in metal concentration because of augmented exposure of active sites to excess  $\text{Cr}^{6+}$  ions.

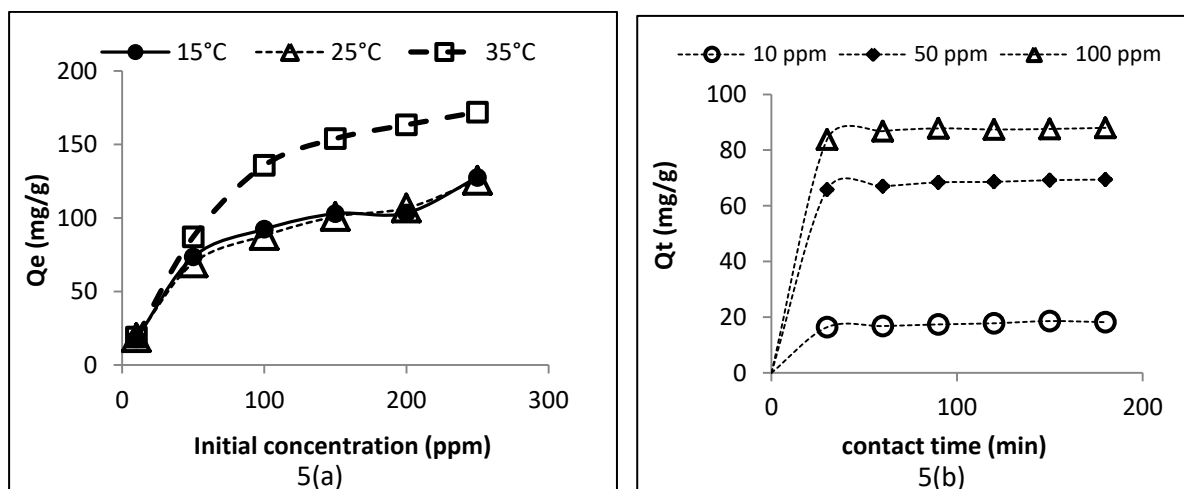


**Fig 5:** Effect of change in (a) adsorbate concentration and (b) contact time on adsorption of  $\text{Cr}^{6+}$  ions on SABP adsorbent.

Adsorption isotherm provides a mathematical expression which relates the variation in equilibrium metal loading over adsorbent as a function of concentration of metal solution. It is a powerful tool which helps in understanding the interaction between metal ions and adsorbent surface (Medhi *et al.*, 2020). Adsorption isotherm study was carried out using 0.1g of SABP adsorbent in 200ml of Cr(VI) solutions having concentrations 10, 50, 100, 150, 200 and 250 ppm respectively at pH = 2. The obtained experimental data was fitted to Langmuir, Freundlich and Redlich-Peterson isotherm models. Graphical representations of these isotherms have been depicted in Figures 6 and 7. The values of corresponding isotherm parameters have been listed in Table 2.

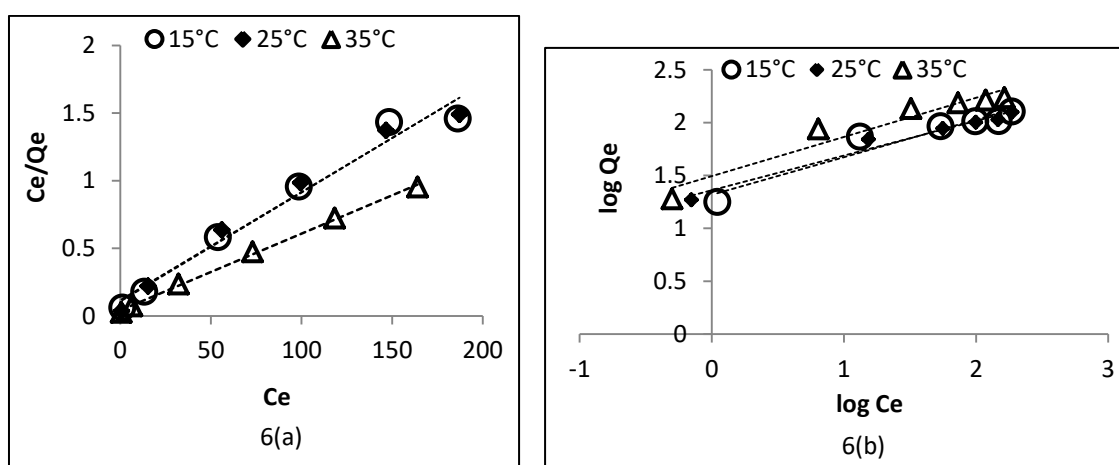


Fig 6: (a) Langmuir and (b) Freundlich isotherms for adsorption of Cr<sup>6+</sup> ions on SABP.

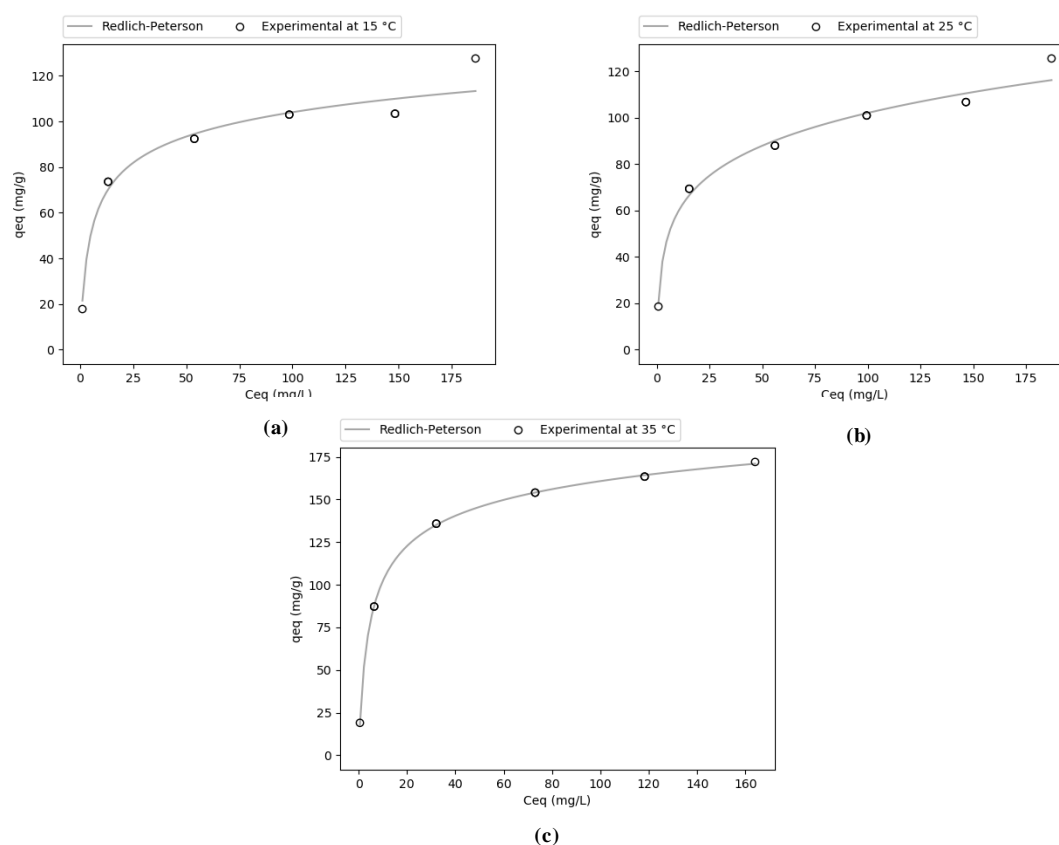


Fig 7: Redlich Peterson isotherms for adsorption of Cr<sup>6+</sup> ions on SABP at (a) 15°C (b) 25°C and (c) 35°C

Langmuir isotherm model is mainly suitable for establishing chemical interactions between the functional groups over the biosorbent surface and the metal ions, resulting in monolayer adsorption. It assumes homogeneous nature of adsorbent surface with no mutual interactions between adsorbed ions on adjacent sites (Mustapha *et al.*, 2019).

**Table 2:** Isotherm parameters for the adsorption of Cr<sup>6+</sup> ions over SABP.

Isotherm models	15°C	25°C	35°C
<i>Langmuir Isotherm</i>			
Q <sub>m</sub> (mg/g)	123.4	125.0	175.4
b (l/mg)	0.076	0.068	0.136
R <sub>L</sub>	0.181	0.194	0.122
R <sup>2</sup>	0.9737	0.9775	0.9981
χ <sup>2</sup>	12.4237	32.9113	6.5078
<i>Freundlich Isotherm</i>			
K <sub>f</sub> (mg/g)(l/mg) <sup>1/n</sup>	20.76	22.94	31.16
n	2.82	3.04	2.69
R <sup>2</sup>	0.9251	0.9736	0.9295
χ <sup>2</sup>	10.5083	4.5351	24.0450
<i>Redlich-Peterson</i>			
A (l/g)	29.2796	58.6326	43.7396
B (l/mg)	0.4569	1.3927	0.4100
β	0.8868	0.8038	0.9027
R <sup>2</sup>	0.9572	0.9817	0.9997
χ <sup>2</sup>	3.6518	1.4806	0.0929

Following linear equation can be used to mathematically express the Langmuir isotherm model:

$$\frac{C_e}{Q_e} = \frac{1}{b \cdot Q_m} + \frac{C_e}{Q_m}$$

where the variables Q<sub>m</sub> and Q<sub>e</sub> denote the maximum monolayer adsorption (mg/g) and the adsorption capacity (mg/g) at equilibrium respectively. Similarly ‘b’ represents a constant which is related to the heat of adsorption. Values of these parameters were evaluated using the slope and intercept of the plot C<sub>e</sub>/Q<sub>e</sub> versus C<sub>e</sub> (Figure 6a). The feasibility of the biosorption process may be reflected by a dimensionless separation factor R<sub>L</sub> which may be computed using following equation:

$$R_L = \frac{1}{1 + b \cdot C_0}$$

where C<sub>0</sub> is the initial concentration of metal solution. Value of R<sub>L</sub> within the range 0 < R<sub>L</sub> < 1 indicates favorable biosorption while the values R<sub>L</sub> = 1, R<sub>L</sub> = 0 and R<sub>L</sub> > 1 suggest linear, irreversible and unfavorable biosorption respectively. It is evident from Table 2 that in the current study, the range of R<sub>L</sub> values (0.122 – 0.194) lie well within 0 to 1, thus revealing favorable biosorption of Cr<sup>6+</sup> ions over SABP.

The Freundlich Isotherm model is an empirical relation between the adsorption capacity (Q<sub>e</sub>) and the metal ion concentration (C<sub>e</sub>) at equilibrium. It is suitable for modeling adsorption over heterogeneous surface having different active sites with varied energies (Mustapha *et al.*, 2019). This model may be expressed by following linear equation:

$$\ln Q_e = \ln K_f + \frac{1}{n} \ln C_e$$

where  $K_f$  and  $n$  are Freundlich constants related to biosorption capacity and the degree of heterogeneity of the biosorbent respectively (**Medhi et al., 2020**). These parameters were obtained from slope and intercept of the plot  $\ln Q_e$  versus  $\ln C_e$  (Figure 6b). The feasibility of the model may be indicated by values of  $n$  within the range  $1 < n < 10$  (**Pandey & Mishra, 2020; Medhi et al., 2020**). The range of values obtained for  $n$  (2.69 – 3.04) in the current study (Table 2) reflect favorable nature of adsorption.

Several studies suggest that adsorption process can be better explained by the Redlich-Peterson (R-P) isotherm model which incorporates three parameters (**Kumara et al., 2014; Morales-Barrera et al., 2020**). This model can be expressed mathematically as follows:

$$Q_e = \frac{A \cdot C_e}{1 + B \cdot C_e^\beta}$$

where  $A$  (l/g) and  $B$  (l/mg) are constants, while  $\beta$  is the exponent having values between 0 and 1. Thus the R-P model combines the characteristic features of Langmuir and Freundlich isotherm models and the equilibrium adsorption capacity ( $Q_e$ ) depends linearly and exponentially on concentration ( $C_e$ ) in numerator and denominator respectively. Depending on the values of  $\beta$ , the adsorption may follow Langmuir model (when  $\beta = 1$ ) and Freundlich model (when the  $\beta$  value tends to zero). The R-P model is thus applicable to both homogeneous and heterogeneous adsorbent surfaces and the adsorption process may not ideally follow formation of monolayer as in case of Langmuir model (**Pakade et al., 2017**). The model can also be expressed by following linear equation:

$$\ln\left(A \cdot \frac{C_e}{Q_e} - 1\right) = \beta \cdot \ln C_e + \ln B$$

Since the equation involves three parameters, the values of these parameters cannot be obtained from linear plot of  $\ln\left(A \cdot \frac{C_e}{Q_e} - 1\right)$  versus  $\ln C_e$  (**Kumar, 2007**). Therefore, the data was analyzed using non-linear regression method with help of CAVS – Adsorption Evaluation Software, version 2.0 (Federal University of Paraná, Curitiba, Paraná, Brazil).

It is evident from Table 2 that all three models exhibited good correlation at temperatures 15°C, 25°C and 35°C with  $R^2$  values  $> 0.9$ , thus the actual mechanism of adsorption may be better expressed by Redlich-Peterson model as a combination of Langmuir and Freundlich models. In order to validate the suitability of Redlich-Peterson model, the deviation between the predicted model data and the experimental data was observed using Chi-square goodness of fit test as follows:

$$\chi^2 = \frac{\sum (Q_e - Q_{e,m})^2}{Q_{e,m}}$$

where  $Q_e$  and  $Q_{e,m}$  are the adsorption capacities (mg/g) at equilibrium, obtained through experiment and isotherm models respectively. Among Langmuir and Freundlich models, the value of  $\chi^2$  static was lower for Langmuir model at 35°C, however at temperatures 15°C and 25°C, the Freundlich model exhibited a lower value of  $\chi^2$  static. On the other hand, compared to other models, the Redlich-Peterson model showed lowest values for  $\chi^2$  static at

temperatures 15°C, 25°C as well as 35°C. This reveals that the experimental data accurately follows the Redlich-Peterson isotherm model. However since the values of the exponent  $\beta$  (0.8038 – 0.9027) lies close to 1, the adsorption is more inclined towards Langmuir model.

The adsorption kinetic study illustrates the time progress of the solute uptake by the adsorbent, which is essential for providing an insight into the actual mechanistic pathway of the adsorption process (Unuabonah *et al.*, 2019). Pseudo first order and pseudo second order models were employed to examine the obtained data and the corresponding graphs have been represented in **Figure 8 (a)** and **(b)** respectively. The kinetic parameters associated with these models have been illustrated in **Table 3**.

In case of pseudo first order kinetics, assuming reversible adsorption of non-dissociable species over the adsorbent surface, the adsorption may be explained by Lagergen (1898) as follows:

$$\frac{dQ_t}{dt} = k_1 \cdot (Q_e - Q_t)$$

where  $k_1$  is the rate constant ( $\text{min}^{-1}$ ). Similarly  $Q_e$  and  $Q_t$  are the adsorption capacities (mg/g) at equilibrium and time  $t$  respectively. The linear equation for this model may be obtained by integration followed by application of boundary conditions  $t = 0$  to  $t$  and  $Q_t = 0$  to  $Q_t$  as follows:  $\log(Q_e - Q_t) = \log Q_e - \frac{k_1 t}{2.303}$

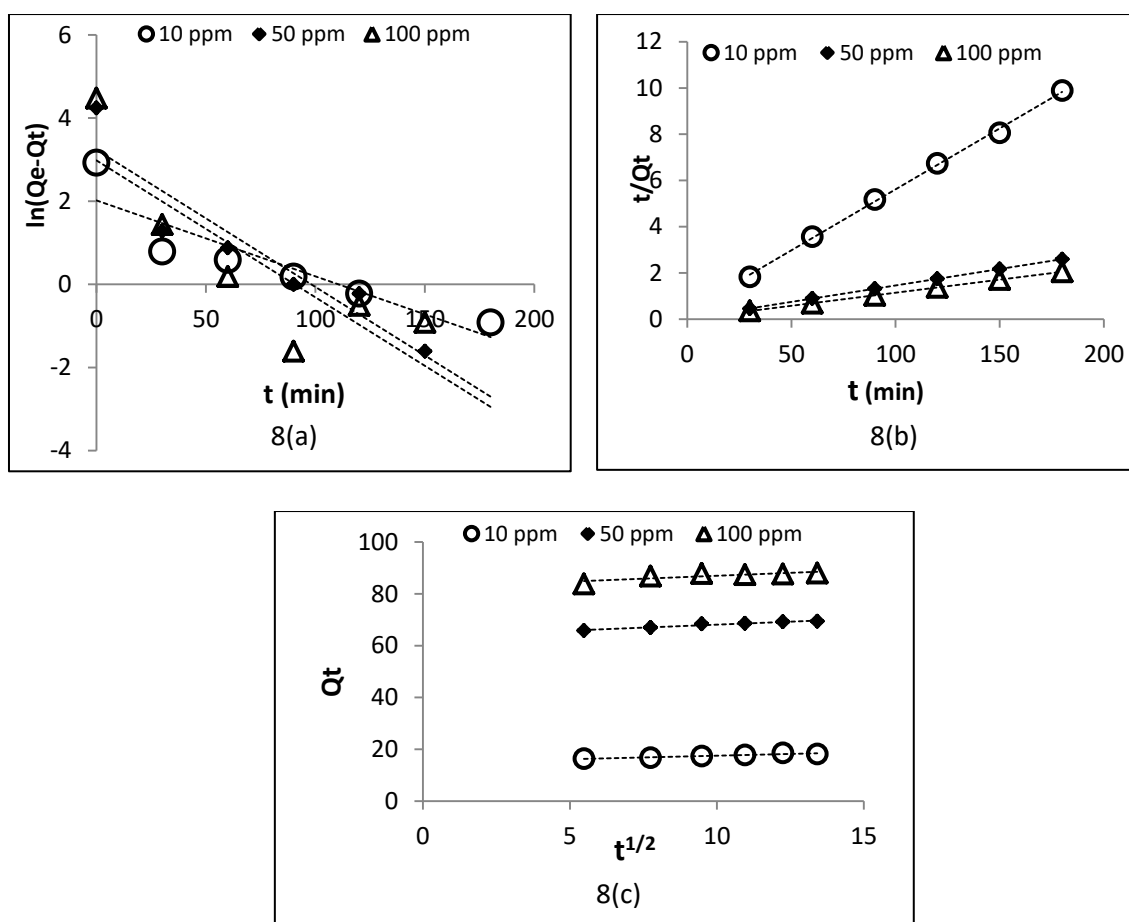


**Fig 8:** (a) Pseudo- first order (b) Pseudo- second order and (c) Intra-particle diffusion kinetic models for adsorption of Cr<sup>6+</sup> ions on SABP

**Table 3:** Kinetic parameters for the adsorption of Cr<sup>6+</sup> ions over SABP.

Kinetic models	10 ppm	50 ppm	100 ppm
<i>Pseudo First Order</i>			
Q <sub>e</sub> (observed) (mg/g)	18.6	69.4	88.0
Q <sub>e</sub> (calculated) (mg/g)	104.5	1715.9	957.19
k <sub>1</sub> (min <sup>-1</sup> )	0.042	0.076	0.076
R <sup>2</sup>	0.8181	0.8764	0.7045
χ <sup>2</sup>	0.7824	0.2595	0.2990
<i>Pseudo Second Order</i>			
Q <sub>e</sub> (observed) (mg/g)	18.6	69.4	88.0
Q <sub>e</sub> (calculated) (mg/g)	19.3	70.4	88.5
k <sub>2</sub> (g/mg/min)	0.00646	0.00551	0.00778
R <sup>2</sup>	0.9986	0.9988	0.9994
χ <sup>2</sup>	0.3276	0.1134	0.0366
<i>Intraparticle diffusion</i>			
k <sub>id</sub> (mg/g/min <sup>1/2</sup> )	0.2716	0.4635	0.4519
C (mg/g)	14.848	63.484	82.432
t <sub>1/2</sub> (s)	499.2	476.4	87.6
D <sub>p</sub> (cm <sup>2</sup> /s)	1.736 x 10 <sup>-9</sup>	1.819 x 10 <sup>-9</sup>	9.894 x 10 <sup>-9</sup>
R <sup>2</sup>	0.9156	0.9570	0.7151
χ <sup>2</sup>	0.0162	0.0061	0.0409

The kinetic parameters for this model were obtained by plot of  $\log(Q_e - Q_t)$  versus  $t$  (Figure 8 a). The y-intercept corresponds to the theoretically predicted value of equilibrium adsorption capacity ( $Q_{e,m}$ ) for this model. Large deviations of  $Q_{e,m}$  from the experimental adsorption capacity ( $Q_e$ ) suggests that the adsorption of Cr<sup>6+</sup> ion on SABP does not follow pseudo first order kinetics.

Several studies have also reported that the adsorption process may follow a pseudo second order kinetic model which may be expressed as:

$$\frac{dQ_t}{dt} = k_2 \cdot (Q_e - Q_t)^2$$

where  $k_2$  is the rate constant (g/mg/min) (Yasemin & Zeki, 2007). Integrating this equation for boundary conditions  $t = 0$  to  $t$  and  $Q_t = 0$  to  $Q_t$  yields a linear form given by:

$$\frac{t}{Q_t} = \frac{1}{Q_e^2} + \frac{t}{Q_e}$$

Plotting  $t/Q_t$  as a function of  $t$ , the kinetic parameters for this model were obtained from the values of slope and intercept. The predicted values of equilibrium adsorption capacity ( $Q_{e,m}$ ) for this model were close to the experimental values ( $Q_e$ ) which indicates that the data followed pseudo second order kinetic model. This observation was further confirmed by the fact that the coefficients of determination ( $R^2$  values) for pseudo second order model were greater than 0.9, in contrast to the pseudo first order model.

Validation of pseudo second order kinetic model was further performed with help of Chi-square test for goodness of fit as follows:

$$\chi^2 = \frac{\sum (Q_t - Q_{t,m})^2}{Q_{t,m}}$$

where  $Q_t$  and  $Q_{t,m}$  are the adsorption capacities obtained via experiments and kinetic models respectively. Significantly low values of  $\chi^2$  for pseudo second order model clearly indicates that the data correlates well with the pseudo second order kinetic model.

The metal ions may undergo diffusion from solvent phase to the adsorbent surface in a number of ways including either film diffusion, pore diffusion, surface diffusion or a suitable combination of these steps (Arris *et al.*, 2016). The exact mechanism of diffusion may be revealed by the intraparticle diffusion model given by following equation:

$$Q_t = k_{id} \cdot t^{1/2} + C$$

where  $k_{id}$  is the rate constant ( $\text{mg/g/min}^{1/2}$ ) while  $C$  is a constant which decides the boundary layer thickness involved in the process (Doke & Khan, 2017). Plot of  $Q_t$  versus  $t^{1/2}$  gives significant information regarding the actual rate determining step. Usually a multi-linear plot suggests involvement of two or more than two diffusion pathways, however a straight line plot passing through the origin indicates that the adsorption mechanism is entirely controlled by intraparticle diffusion (Arris *et al.*, 2016; Medhi *et al.*, 2020).

The role of intraparticle pore diffusion may further be investigated by evaluating the pore diffusion coefficient  $D_p$  ( $\text{cm}^2/\text{s}$ ) which is given by the following equation:

$$D_p = \frac{0.03 r_0^2}{t_{1/2}}$$

where  $r_0$  is the radius (cm) of biosorbent particle while  $t_{1/2}$  is the half-life period (s) for the adsorption process (Sathishkumar *et al.*, 2009).  $D_p$  values within the range  $10^{-11}$  to  $10^{-13}$   $\text{cm}^2/\text{s}$  suggest that the rate determining step involves intraparticle pore diffusion (Doke & Khan, 2017). In the present study, the  $D_p$  values were evaluated assuming the average particle diameter as  $107.5\mu\text{m}$  which gives the  $r_0$  value equal to  $5.375 \times 10^{-3}$  cm. Similarly the  $t_{1/2}$  value was calculated with help of pseudo second order rate constant ( $k_2$ ) using the equation (Karthikeyan *et al.*, 2010):

$$t_{1/2} = \frac{1}{k_2 \cdot Q_e}$$

**Figure 8(c)** depicts the plots obtained for intraparticle diffusion model. The corresponding parameters including the  $t_{1/2}$  and  $D_p$  values have been listed in **Table 3**. Although the plots obtained for  $Q_t$  versus  $t^{1/2}$  were fairly linear ( $R^2 > 0.7$ ), these plots deviated from the origin and exhibited large values of the intercept ( $C$ ). Such observation clearly indicates that the process was not entirely controlled by pore diffusion mechanism and there exists significant contribution of the surface sorption (Arris *et al.*, 2016; Doke & Khan, 2017; Medhi *et al.*, 2020). This observation was further validated by the  $D_p$  values which lie in the order  $10^{-9}$   $\text{cm}^2/\text{s}$ .

Thermodynamic study was conducted by evaluating various thermodynamic parameters such as free energy change ( $\Delta G$ ), change in enthalpy ( $\Delta H$ ) and the change in entropy ( $\Delta S$ ) during the adsorption process. Determination of these parameters gives important information regarding the feasibility and mechanism of the adsorption process (Liu *et al.*, 2007). As evident from Table 2, the increase in temperature from  $15^\circ\text{C}$  to  $35^\circ\text{C}$  enhanced monolayer

adsorption capacity ( $Q_m$ ) from 123.4 to 175.4 mg/g which reflects the endothermic nature of the process.

Thermodynamic parameters were evaluated with help of the thermodynamic equilibrium constant  $K$ , which was estimated using the method adopted by **Liu *et al.* (2007)** and **Yasemin & Zeki (2007)**. **Figure 9a** displays plots of  $\ln(Q_e/C_e)$  as a function of  $Q_e$  at temperatures 15°C, 25°C and 35°C respectively, where  $Q_e$  and  $C_e$  represent adsorption capacity (mg/g) and the adsorbate concentration (mg/l) at equilibrium. The y-intercept of these plots yields  $K$  at respective temperatures. Using these values of  $K$ , the thermodynamic parameters were evaluated from the intercept and slope of the plot  $\ln K$  versus  $1/T$  (**Figure 9b**) with help of following Vant Hoff equation (**Liu *et al.*, 2018**):

$$\Delta G = -RT \ln K$$

$$\ln K = \frac{\Delta S}{R} - \frac{\Delta H}{RT}$$

where the gas constant  $R = 8.314 \times 10^{-3}$  kJ/K/mol and  $T$  is the temperature in kelvins. The parameters thus computed have been listed in **Table 4**.

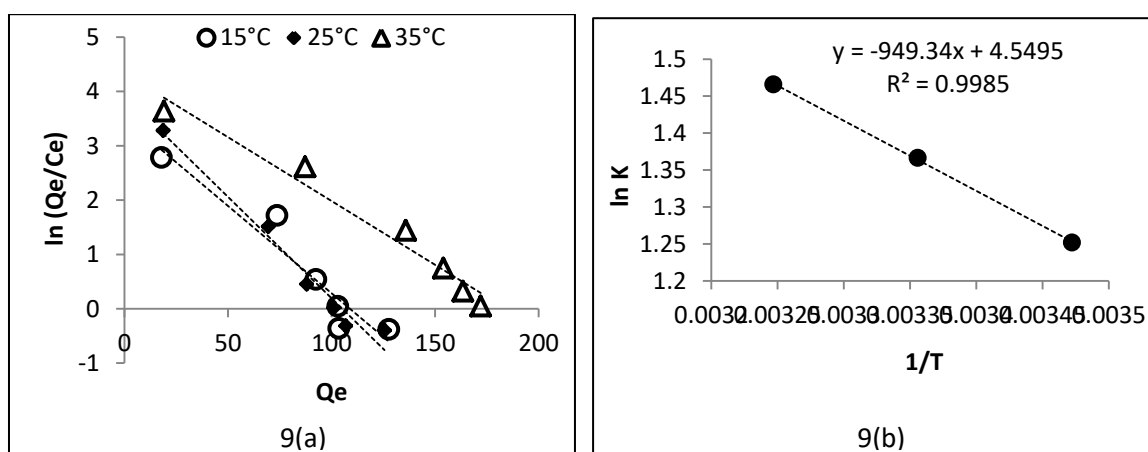


**Fig 9:** (a) Plot of  $\ln(Q_e/C_e)$  versus  $Q_e$  and (b) Vant Hoff plot for adsorption of  $\text{Cr(VI)}$  ions on SABP

**Table 4:** Thermodynamic parameters for the adsorption of  $\text{Cr}^{6+}$  ions over SABP.

Temperature (K)	K	$\Delta G$ (kJ/mol)	$\Delta H$ (kJ/mol)	$\Delta S$ (J/K/mol)
288	3.4971	-3.0		
298	3.9216	-3.4	7.9	37.8
308	4.3314	-3.7		

$\Delta H$  and  $\Delta S$  values for  $\text{Cr}^{6+}$  adsorption over SABP were 7.9 kJ/mol and 37.8 J/K/mol respectively. Positive values of  $\Delta H$  further support the endothermic nature of the adsorption. Similarly positive values of  $\Delta S$  reveal randomness of the adsorption process at the adsorbate – adsorbent interface. On the other hand,  $\Delta G$  exhibited negative values which further decreased with increase in temperature, indicating spontaneous nature of the process.

Thus, the adsorption of  $\text{Cr}^{6+}$  ions over SABP may be attributed mainly to the interaction of functional groups specifically, the hydroxyl group with  $\text{Cr}^{6+}$  ions. Several components of *Saraca asoca* bark including cellulose, hemicellulose and lignin may provide a number of hydroxyl groups directly attached to the surface of SABP particle. The biosorption of  $\text{Cr}^{6+}$  over SABP occurs mainly in acidic medium. Since in acidic medium,  $\text{Cr}^{6+}$  exists in the form

of  $\text{HCrO}_4^-$  anion, the electrostatic attraction between  $\text{HCrO}_4^-$  and the protonated hydroxyl groups of SABP results in biosorption of  $\text{Cr}^{6+}$  ions. This interaction was clearly revealed by the FTIR spectra which displayed shifting of O-H stretching frequency in Cr-loaded SABP. The isotherm study suggests that the adsorption process may not be limited to formation of monolayer. Moreover, the diffusion mechanism involved substantial roles of surface diffusion as well as pore diffusion. The schematic representation of the overall biosorption mechanism has been depicted in **Figure 10**.

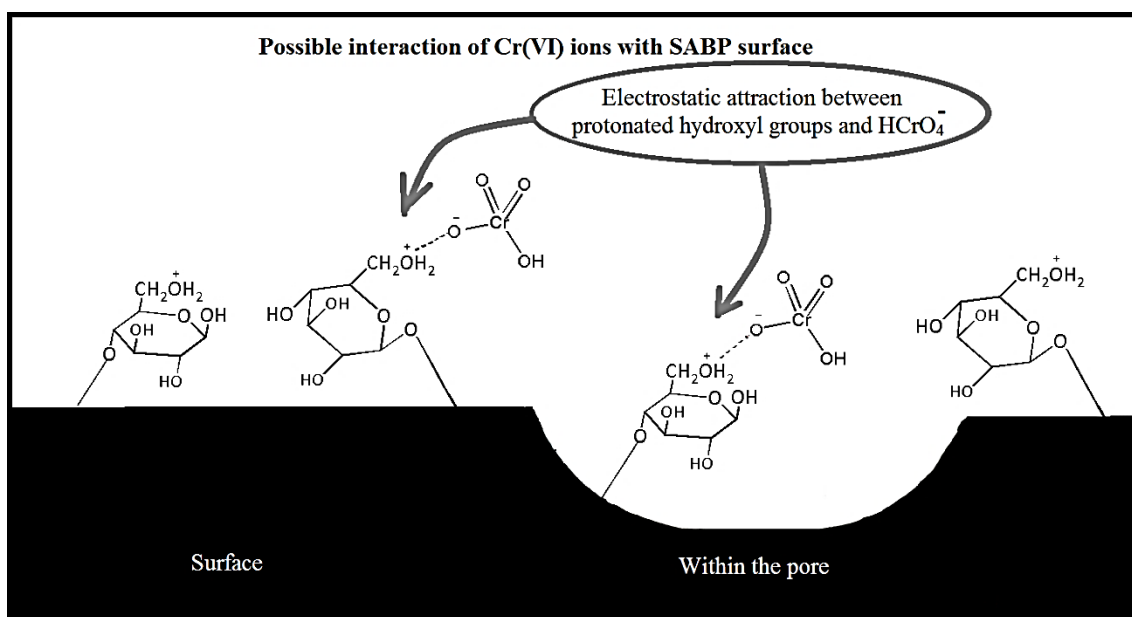


**Fig 10:** Schematic representation of the mechanism for biosorption of Cr(VI) over SABP

**Table 5** compares the adsorption capacities of various biosorbents reported in literature for Cr(VI) remediation. The dissimilarities in various treatment procedures and related experimental set-up complicate the comparison of biosorbents. Therefore the Langmuir model monolayer biosorption capacities ( $Q_m$ ) were used for comparison of biosorbents. In the present study, at pH 2.0 and 25°C temperature, the observed  $Q_m$  value = 125.0 mg/g which is comparable to those reported in other studies.

**Table 5:** Comparison of adsorption capacities for various biosorbents reported in literature

Biosorbent	Maximum adsorption capacity (mg/g)	Optimum pH	Reference
Pine needles	5.36	2.0	Dakiky <i>et al.</i> , 2002
Coconut husk fibers	29.0	2.1	Tan <i>et al.</i> , 1993
Eucalyptus bark	45.0	2.0	Sarin & Pant., 2006
Cross-linked chitosan	78.0	5.0	Schmuhl <i>et al.</i> , 2001
<i>Portulaca oleracea</i>	54.95	2.0	Mishra <i>et al.</i> , 2015
Gum kondagogu	129.8	2.0	Vinod <i>et al.</i> , 2010
Bagasse fly-ash	260	1.0	Gupta <i>et al.</i> , 1999
<i>Cupressus lusitanica</i> bark	305.4	1.5	Netzahuatl-Munoz <i>et al.</i> , 2015
<i>Saraca asoca</i> bark powder (SABP)	125.0	2.0	Present Study

## CONCLUSION

*Saraca asoca* trees are found in different parts of South Asia. The bark powder of *Saraca asoca* tree (SABP) may prove to be useful as a low cost biosorbent. The biosorption of Cr(VI) over SABP was found to be dependent on various experimental conditions such as pH, contact time, initial Cr(VI) concentration and temperature. SABP is reasonably good for Cr(VI) adsorption in acidic medium. The hydroxyl groups on the biosorbent surface easily acquire positive charge in acidic medium and thus are able to interact electrostatically with negatively charged chromium species. The shifts in –OH peaks of FTIR spectra confirmed this interaction. At pH 2.0 and temperature 25°C, using adsorbent dose 0.5 g/l, the maximum Cr(VI) biosorption capacity was 125.0 mg/g. Modeling of biosorption equilibrium revealed that the data efficiently followed the Redlich-Peterson isotherm model. Similarly the biosorption kinetics was well explained by the pseudo-second order model and the diffusion of solute was influenced by surface as well as pore diffusion mechanisms. The thermodynamic parameters demonstrated endothermic and spontaneous nature of biosorption. Thus considering its non-toxic nature and low cost, the *Saraca asoca* bark powder may be useful as a potent cost-effective Cr(VI) biosorbent.

## ACKNOWLEDGEMENT

Authors gratefully acknowledge the Vice-Chancellor and the Head of Chemistry Department, Sam Higginbottom University of Agriculture, Technology and Sciences, Prayagraj, UP, India, for providing necessary facilities to carry out this research work.

## GRANT SUPPORT DETAILS

The present research did not receive any financial support.

## CONFLICT OF INTEREST

The authors declare that there is no conflict of interests regarding the publication of this manuscript. In addition, the ethical issues, including plagiarism, informed consent, misconduct, data fabrication and/ or falsification, double publication and/or submission, and redundancy has been completely observed by the authors.

## LIFE SCIENCE REPORTING

No life science threat was practiced in this research.

## REFERENCES

- Ahmad, F., Misra, L., Tewari, R., Gupta, P., Mishra, P. and Shukla, R. (2016). Anti-inflammatory flavanol glycosides from *Saraca asoca* bark. *Natural product research*, 30(4); 489-492.
- Ajmani, A., Shahnaz, T., Subbiah, S. and Narayanasamy, S. (2019). Hexavalent chromium adsorption on virgin, biochar, and chemically modified carbons prepared from *Phaneravahlii* fruit biomass: equilibrium, kinetics, and thermodynamics approach. *Environmental Science and Pollution Research*, 26(31); 32137-32150.
- Alemu, A., Lemma, B., Gabbiye, N., Alula, M. T. and Desta, M. T. (2018). Removal of chromium (VI) from aqueous solution using vesicular basalt: a potential low cost wastewater treatment system. *Heliyon*, 4(7); e00682.

- Arris, S., Lehocine, M. B. and Meniai, A. H. (2016). Sorption study of chromium sorption from wastewater using cereal by-products. *International journal of hydrogen energy*, 41(24); 10299-10310.
- Bhattacharya, A. K., Naiya, T. K., Mandal, S. N., Das, S. K. (2008) Adsorption, kinetics and equilibrium studies on removal of Cr (VI) from aqueous solutions using different low-cost adsorbents. *Chemical Engineering Journal*, 137(3); 529-541.
- Campaña-Pérez, J. F., Barahona, P. P., Martín-Ramos, P. and Barriga, E. J. C. (2019). Ecuadorian yeast species as microbial particles for Cr (VI) biosorption. *Environmental Science and Pollution Research*, 26(27); 28162-28172.
- Chen, H., Dai, G., Zhao, J., Zhong, A., Wu, J. and Yan, H. (2010). Removal of copper (II) ions by a biosorbent—*Cinnamomum camphora* leaves powder. *Journal of Hazardous Materials*, 177(1-3); 228-236.
- Coates, J. (2000). Interpretation of infrared spectra, a practical approach. *Encyclopedia of Analytical Chemistry*, R.A. Meyers (Ed.) John Wiley & Sons Ltd. pp. 10815–10837.
- Dada, A. O., Adekola, F. A., Odebunmi, E. O., Dada, F. E., Bello, O. M., Akinyemi, B. A., ... and Umukoro, O. G. (2020). Sustainable and low-cost *Ocimum gratissimum* for biosorption of indigo carmine dye: kinetics, isotherm, and thermodynamic studies. *International Journal of Phytoremediation*, 22(14); 1524-1537.
- Dakiky, M., Khamis, M., Manassra, A. and Mer'Eb, M. (2002). Selective adsorption of chromium (VI) in industrial wastewater using low-cost abundantly available adsorbents. *Advances in environmental research*, 6(4); 533-540.
- Doke, K. M. and Khan, E. M. (2017). Equilibrium, kinetic and diffusion mechanism of Cr (VI) adsorption onto activated carbon derived from wood apple shell. *Arabian journal of chemistry*, 10; S252-S260.
- Fuks, L., Filipiuk, D. and Majdan, M. (2006). Transition metal complexes with alginate biosorbent. *Journal of Molecular Structure*, 792; 104-109.
- Gebrehawaria, G., Hussen, A. and Rao, V. M. (2015). Removal of hexavalent chromium from aqueous solutions using barks of *Acacia albida* and leaves of *Eucleaschimperi*. *International Journal of Environmental Science and Technology*, 12(5); 1569-1580.
- Gómez-Aguilar, D. L., Rodríguez-Miranda, J. P., Baracaldo-Guzmán, D., Salcedo-Parra, O. J. and Esteban-Muñoz, J. A. (2021). Biosorption of Pb (II) Using Coffee Pulp as a Sustainable Alternative for Wastewater Treatment. *Applied Sciences*, 11(13); 6066.
- Gupta, V. K., Mohan, D., Sharma, S. and Park, K. T. (1998). Removal of chromium (VI) from electroplating industry wastewater using bagasse fly ash—a sugar industry waste material. *Environmentalist*, 19(2); 129-136.
- Hadjmohammadi, M. R., Salary, M. and Biparva, P. (2011). Removal of Cr (VI) from aqueous solution using Pine Needles Powder as a biosorbent. *Journal of Applied Sciences in Environmental Sanitation*, 6(1); 1-13.
- Karthik, R. and Meenakshi, S. (2014). Removal of hexavalent chromium ions using polyaniline/silica gel composite. *Journal of Water Process Engineering*, 1; 37-45.
- Karthikeyan, S., Sivakumar, B. and Sivakumar, N. (2010). Film and pore diffusion modeling for adsorption of reactive red 2 from aqueous solution on to activated carbon prepared from bio-diesel industrial waste. *E-Journal of Chemistry*, 7(S1); S175-S184.
- Kavitha, V. U. and Kandasubramanian, B. (2020). Tannins for wastewater treatment. *SN Applied Sciences*, 2; 1-21.
- Kumar, K. V. (2007). Optimum sorption isotherm by linear and non-linear methods for malachite green onto lemon peel. *Dyes and pigments*, 74(3); 595-597.
- Kumara, N. T. R. N., Hamdan, N., Petra, M. I., Tennakoon, K. U. and Ekanayake, P. (2014). Equilibrium isotherm studies of adsorption of pigments extracted from *Kuduk-kuduk* (*Melastoma malabathricum* L.) pulp onto TiO<sub>2</sub> nanoparticles. *Journal of Chemistry*, 2014; 1-6.
- Lagergren, S. (1898). Ueber die Dämpfung elektrischer resonatoren. *Annalen der Physik*, 300(2); 290-314.
- Lazarević, S., Janković-Častvan, I., Jovanović, D., Milonjić, S., Janačković, D. and Petrović, R. (2007). Adsorption of Pb<sup>2+</sup>, Cd<sup>2+</sup> and Sr<sup>2+</sup> ions onto natural and acid-activated

- sepiolites. *Applied Clay Science*, 37(1-2); 47-57.
- Litefti, K., Freire, M. S., Stitou, M. and González-Álvarez, J. (2019). Adsorption of an anionic dye (Congo red) from aqueous solutions by pine bark. *Scientific Reports*, 9(1); 1-11.
- Liu, Y., Xiao, D. and Li, H. (2007). Kinetics and thermodynamics of lead (II) adsorption on vermiculite. *Separation Science and Technology*, 42(1); 185-202.
- Liu, Q., Li, T., Zhang, S., Qu, L. and Ren, B. (2018). Optimization and evaluation of alkali-pretreated *Paonia ostii* seed coats as adsorbent for the removal of MB from aqueous solution. *Polish Journal of Chemical Technology*, 20(3); 29-36.
- Ma, Y., Liu, W. J., Zhang, N., Li, Y. S., Jiang, H. and Sheng, G. P. (2014). Polyethylenimine modified biochar adsorbent for hexavalent chromium removal from the aqueous solution. *Bioresource technology*, 169; 403-408.
- Medhi, H., Chowdhury, P. R., Baruah, P. D. and Bhattacharyya, K. G. (2020). Kinetics of Aqueous Cu (II) Biosorption onto *Thevetiaperuviana* Leaf Powder. *ACS omega*, 5(23); 13489-13502.
- Mishra, A., Dubey, A. and Shinghal, S. (2015). Biosorption of chromium (VI) from aqueous solutions using waste plant biomass. *International Journal of Environmental Science and Technology*, 12(4); 1415-1426.
- Mohebbali, S., Bastani, D. and Shayesteh, H. (2019). Equilibrium, kinetic and thermodynamic studies of a low-cost biosorbent for the removal of Congo red dye: acid and CTAB-acid modified celery (*Apium graveolens*). *Journal of Molecular Structure*, 1176; 181-193.
- Morales-Barrera, L., Flores-Ortiz, C. M. and Cristiani-Urbina, E. (2020). Single and binary equilibrium studies for Ni<sup>2+</sup> and Zn<sup>2+</sup> biosorption onto *lemna gibba* from aqueous solutions. *Processes*, 8(9); 1089.
- Mukhopadhyay, M. K. and Nath, D. (2011). Phytochemical screening and toxicity study of *Saraca asoca* bark methanolic extract. *International Journal of Phytomedicine*, 3(4); 498.
- Mustapha, S., Shuaib, D. T., Ndamitso, M. M., Etsuyankpa, M. B., Sumaila, A., Mohammed, U. M. and Nasirudeen, M. B. (2019). Adsorption isotherm, kinetic and thermodynamic studies for the removal of Pb (II), Cd (II), Zn (II) and Cu (II) ions from aqueous solutions using *Albizia lebeck* pods. *Applied water science*, 9(6); 1-11.
- Mutongo, F., Kuipa, O. and Kuipa, P. K. (2014). Removal of Cr (VI) from aqueous solutions using powder of potato peelings as a low cost sorbent. *Bioinorganic chemistry and applications*, 2014.
- Netzahuatl-Muñoz, A. R., Cristiani-Urbina, M. D. C. and Cristiani-Urbina, E. (2015). Chromium biosorption from Cr (VI) aqueous solutions by *Cupressus lusitanica* bark: Kinetics, equilibrium and thermodynamic studies. *PLoS One*, 10(9); e0137086.
- Ofomaja, A. E. and Ho, Y. S. (2007). Effect of pH on cadmium biosorption by coconut copra meal. *Journal of Hazardous Materials*, 139(2); 356-362.
- Omorogie, M. O., Babalola, J. O., Unuabonah, E. I., Song, W. and Gong, J. R. (2016). Efficient chromium abstraction from aqueous solution using a low-cost biosorbent: *Nauclea diderrichii* seed biomass waste. *Journal of Saudi Chemical Society*, 20(1); 49-57.
- Pakade, V. E., Ntuli, T. D. and Ofomaja, A. E. (2017). Biosorption of hexavalent chromium from aqueous solutions by *Macadamia nutshell* powder. *Applied Water Science*, 7(6); 3015-3030.
- Pandey, A. K. and Mishra, A. K. (2020). Tunable electrochemical synthesis of pyrrole-based adsorbents. *Separation Science and Technology*, 55(18); 3329-3342.
- Politi, D. and Sdiras, D. (2020). Modified spruce sawdust for sorption of hexavalent chromium in batch systems and fixed-bed columns. *Molecules*, 25(21); 5156.
- Saliba, R., Gauthier, H., Gauthier, R. and Petit-Ramel, M. (2002). The use of eucalyptus barks for the adsorption of heavy metal ions and dyes. *Adsorption Science & Technology*, 20(2); 119-129.
- Sarin, V. and Pant, K. (2006). Removal of chromium from industrial waste by using eucalyptus bark. *Bioresource technology*, 97(1); 15-20.
- Sathishkumar, M., Binupriya, A. R., Kavitha, D., Selvakumar, R., Jayabalan, R., Choi, J. G. and Yun, S. E. (2009). Adsorption potential of maize cob carbon for 2, 4-dichlorophenol removal from aqueous solutions: equilibrium, kinetics and thermodynamics modeling. *Chemical Engineering Journal*, 147(2-3); 265-271.
- Saxena, A., Bhardwaj, M., Allen, T., Kumar, S. and Sahney, R. (2017). Adsorption of heavy metals from

- wastewater using agricultural–industrial wastes as biosorbents. *Water Science*, 31(2); 189-197.
- Schmuhl, R., Krieg, H. M. and Keizer, K. (2001). Adsorption of Cu (II) and Cr (VI) ions by chitosan: Kinetics and equilibrium studies. *Water Sa*, 27(1); 1-8.
- Smitha, G. R. and Thondaiman, V. (2016). Reproductive biology and breeding system of *Saraca asoca* (Roxb.) De Wilde: a vulnerable medicinal plant. *Springerplus*, 5(1); 1-15.
- Sud, D., Mahajan, G. and Kaur, M. P. (2008). Agricultural waste material as potential adsorbent for sequestering heavy metal ions from aqueous solutions—A review. *Bioresource technology*, 99(14); 6017-6027.
- Tan, W. T., Ooi, S. T. and Lee, C. K. (1993). Removal of chromium (VI) from solution by coconut husk and palm pressed fibres. *Environmental technology*, 14(3); 277-282.
- Tao, F., Wang, Y., Zhao, Z., Liu, X., Zhang, G., Li, C., ... and Huo, Q. (2020). Effective removal of Cr (VI) in aqueous solutions using *Caulis Ionicerae* residue fermented by *Phanerochaete chrysosporium*. *Preparative Biochemistry & Biotechnology*; 1-10.
- Unuabonah, E. I., Omorogie, M. O. and Oladoja, N. A. (2019). Modeling in adsorption: fundamentals and applications. In *Composite Nanoadsorbents* (pp. 85-118). Elsevier.
- Vinod, V. T. P., Sashidhar, R. B. and Sreedhar, B. (2010). Biosorption of nickel and total chromium from aqueous solution by gum kondagogu (*Cochlospermum gossypium*): A carbohydrate biopolymer. *Journal of hazardous materials*, 178(1-3); 851-860.
- Wang, J. and Chen, C. (2009). Biosorbents for heavy metals removal and their future. *Biotechnology advances*, 27(2); 195-226.
- Yasemin, B. and Zeki, T. (2007). Removal of heavy metals from aqueous solution by sawdust adsorption. *Journal of environmental sciences*, 19(2); 160-166.
- Yuvaraja, G., Krishnaiah, N., Subbaiah, M. V. and Krishnaiah, A. (2014). Biosorption of Pb (II) from aqueous solution by *Solanum melongena* leaf powder as a low-cost biosorbent prepared from agricultural waste. *Colloids and Surfaces B: Biointerfaces*, 114; 75-81.
- Zhou, L., Liu, Y., Liu, S., Yin, Y., Zeng, G., Tan, X., Huang, X. (2016). Investigation of the adsorption-reduction mechanisms of hexavalent chromium by ramie biochars of different pyrolytic temperatures. *Bioresource Technology*, 218; 351-359.